Current steering detection scheme of three terminal antenna coupled terahertz FET detectors

Péter Földesy

Computer and Automation Research Institute, Hungarian Academy of Sciences, Kende utca 13-17, H1111, Budapest, Hungary

Faculty of Information Technology, Péter Pázmány Catholic University, Práter u. 50/a, 1083, Budapest, Hungary

Corresponding author: foldesy.peter@sztaki.mta.hu

Compiled July 3, 2013

Antenna coupled field effect transistor (FET) as plasma wave THz detector is used with current steering to record separately the gate-source, gate-drain photoresponse, and their phase sensitive combination. The method based on the observation that the plasmon-terminal coupling is cut-off in saturation resulting in only one side sensitivity. A polarimetric example is presented with intensity and polarization angle reconstruction using a single three terminal antenna coupled Si-MOSFET. The technique is applicable to various detection schemes and technologies (HEMT, GaAs-, GaN-, Si-MOSFETs) and other application possibilities are discussed.

OCIS codes: 040.2235, 130.5440, 250.0040

Terahertz imaging technologies gained a lot by discovering the plasma wave rectification [1] [2]. The 2D electron plasma of the field effect transistors under their gate terminal provides a simple means to rectify high frequency radiation. Various implementation have appeared using GaAs/AlGaAs high electron mobility transistors, graphene, and GaAs-, GaN-, Si-MOSFETs [3]. Though other exotic approaches may provide better properties, in focal plane solutions, the commercial silicon technology is the common platform. Using optical elements and multiple detectors (e.g. two detector arms) complex properties can be measured beside absorption and reflection parameters, such as phase delay or polarization angle. The distinguishing feature of the introduced method is that a single antenna coupled FET detector is used to measured different radiation properties selected by means of simple electronic control.

First, the FET plasma wave detection is revised briefly. In the conducting channel of a FET a 2D electron sheet is formed as a function of the gate potential. The high frequency (RF) radiation is coupled to the gate and e.g. to the source terminal. The RF signal of the gate modulates the electron density while the source coupled signal is fed into this varying conductivity channel. The resulting behavior is equal to a power-law detector (like a bolometer) that measures the time averaged intensity. With decreasing gate potential, the electron sheet becomes thinner and more sensitive to the RF perturbation, thus the response becomes higher. As the transistor reaches subthreshold region, the photoresponse saturates and driving further the transistor into accumulation region, the response quickly drops as the inversion electron sheet disappears. In a symmetrically connected FET structure, there is no difference between the gate-source and gate-drain coupled signal rectification. At the same RF signal the photoresponses are equal but of opposite sign. The practical difference comes from the electronic and RF connectivity of the FET. The biasing is usually distinguished as open drain and current biased modes. In the former, beside the instrumentation load there is no active element connected to the source or drain terminals. In the current biased mode, non zero source drain current is forced to the transistor. It was demonstrated in various works, that the non zero source-drain current results in significantly higher responsivity, with the connotation of the increasing sensor noise due to $1/f$ flicker and shot noise [4]. Let be u^{ac}_{GS}, u^{ac}_{GD} the gate-source and gate-drain RF signals, than the ΔU_S and ΔU_D photoresponse can be modeled by DC current characteristics as [5]:

$$\Delta U_{S(D)} = \eta_{S(D)} \{u^{ac}_{GS(D)}\}^2 \frac{\partial ln\left[I_{DS}(V_{GS}, V_{DS})\right]}{\partial V_{GS(D)}} \quad (1)$$

$\eta_{S(D)}$ efficiency is derived from the coupling efficiency of the incoming radiation and the impedance of the terminals. The free space radiation is coupled to the terminals usually by antenna or waveguide structures, which primary determines the overall frequency response of the detector in addition to the ideal photoresponse.

The previously not reported observation used thereafter is that in the saturation, the depleted region of the channel cannot constitute to the photoresponse, due to the vanishing carrier concentration ($\partial I_{DS}/\partial V_{GD} \to 0$, hence $\Delta U_{GD} \to 0$). The advantageous consequence is that biasing the transistor into saturation and then swapping the electronic connection of the source and drain, the photoresponse of the terminals can be measured independently. The necessary condition is that the plasma perturbation is cut-off from the terminal by the increasing depleted channel length (pinch-off length). This condition is twofold, first the transistor technology should provide saturation region and the V_{DS} voltage must exceed the pinch-off voltage V_P. For exam-

ple, the silicon MOSFETs can satisfy these conditions. In the most sensitive subthreshold region, the saturation voltage is V_{GS} independent constant and is about $V_P \cong 4V_{th} \cong 100mV$ in room temperature, where V_{th} is the thermal voltage. Hence, relatively easy to eliminate the drain side photoresponse and get solely the gate-source direct detection component. Between the two saturated cases, both side constitute to the measured value with changing weights and opposite sign. In this region another terms appear, namely mixing terms between the gate-source(drain) and drain-source [6]. These terms are proportional to $\Delta U_{mixing} \propto u^{ac}_{GS} u^{ac}_{DS} cos(\varphi)$, where φ is the phase difference in between. Hence, all three regions are distinctively informative. An illustration of these cases is shown in Fig. 1a and typical photoresponse is shown in Fig. 1b as a function of the source-drain voltage V_{DS} at constant V_{GS}.

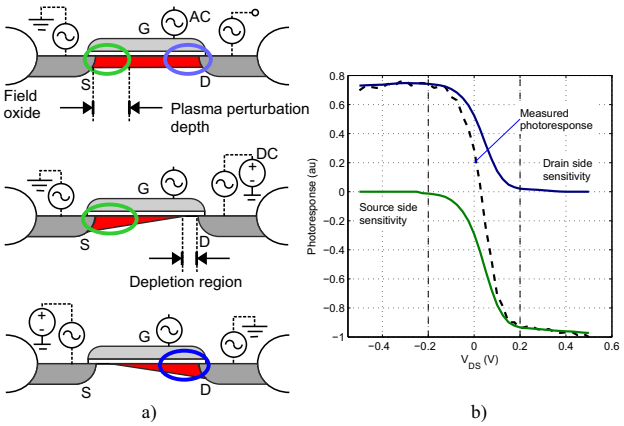

Fig. 1. (Color online) Illustration of the FET plasma wave detector under different biasing conditions (a): (top) no drain-source current flows, the source and drain side have equal responsivity; (middle) the drain side is biased as the depletion region of the channel cuts off the plasma perturbation from the drain, only the source side is sensitive; (bottom) the drain side is sensitive. (b) Modeled responsivity and measured photoresponse as a function of the drain-source potential with fixed gate potential and equal RF signal.

In order to present a practical application of the this measurement method, a cross dipole antenna coupled silicon FET detector is used for polarization imaging. Terahertz polarimetry [7] is selected as it applied widely to analyze birefringent materials [8], metamaterials, not-normal incidence reflection, and multiple scattering samples [9]. The used detector is manufactured in standard $180nm$ feature sized CMOS technology with $440nm$ drawn width and $330nm$ length. The microphoto of the detector and its electronic connection is presented in Fig. 2a,b and Fig. 2c, respectively. Important to note, that the grounded cross-dipole arms introduces asymmetry, resulting in polarization sensitivity similar to the "Y" shaped structure described in [10]. A low noise amplifier is integrated in the circuit providing $40dB$ amplification.

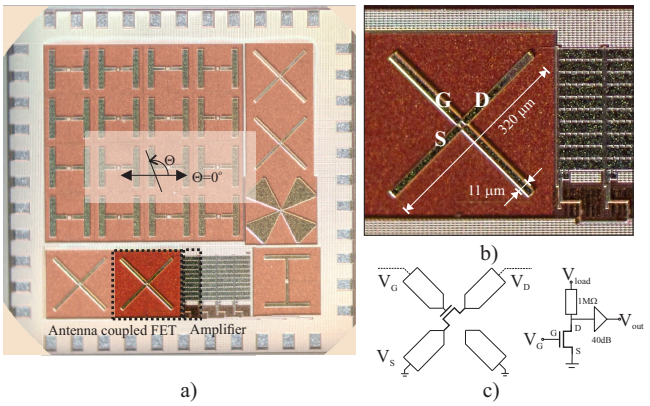

Fig. 2. (Color online) Microphoto of the antenna coupled FET detector chip and the connected amplifier (a). The (b) shows a closeup of the detector used in the experiments. The (c) shows the electronic connection of the used detector.

In the presented measurement example, a resistive load of $1M\Omega$ is used with voltage source (V_{load}) to control the detector FET biasing. The saturated conditions are achieved by positive and negative (V_{load}) values. The detector was situated in an optical table with common building blocks maintaining focusing and polarization (Fig. 4). The radiation source was a VDI CW source operated at $362GHz$ with $0.8mW$ nominal power and the data was captured by standard lock-in technique. First, the polarization dependence had been characterized. The detector was biased into subthreshold saturation and is rotated in 360 degree. At every angle increment, two photoresponses were recorded with constant $V_G = 0.33V$, $1KHz$ modulation frequency, and $10Hz$ acquisition rate. The two saturated cases were set by $V_{load} = \pm 0.5$. The settings resulted in $V_{DS} \cong -140mV$ and $V_{DS} \cong +200mV$ due to voltage drop on the load transistor, driving the transistor into saturation in both cases. The measured polarization angle dependent responses can be seen in Fig. 3a, which shows a sinusoid characteristics with 45^o polarization angle shift between the two recordings. From the recordings, the polarization angle Θ and the polarization independent intensity I can be reconstructed. The response can be fit to:

$$\begin{aligned} \Delta U_D &= \eta_D I\left(cos\left(2\Theta\right) + k_D\right) \\ \Delta U_S &= -\eta_S I\left(sin\left(2\Theta\right) + k_S\right) \end{aligned} \tag{2}$$

where $k_{S(D)}$ are structure and implementation dependent constant values, while $\eta_{S(D)}$ varies also with biasing. The remaining unknowns in Eq. (2) are the intensity and the polarization angle. Their solution is quadratic with ambiguous solution, which can be solved by iterative unwrapping used in phase retrieval [11].

After characterization, a plastic spoon had been placed in the object translation stage (Fig. 4) and raster scanned. The scanning performed point by point in a $40mm$ by $35mm$ area with $0.5mm$ spatial frequency sampling rate. The Fig. 5a shows the visual photo of the

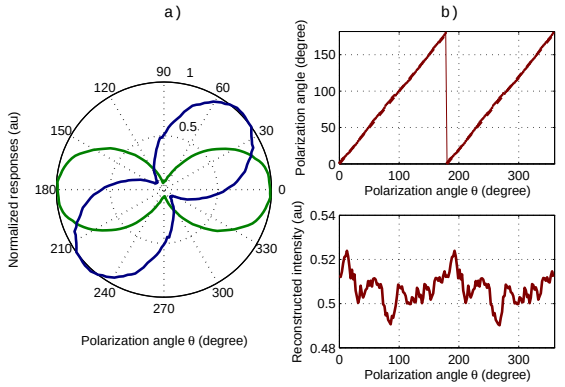

Fig. 3. (Color online) The (a) shows the separately recorded source (green) and drain (blue) side normalized photoresponses as a function of the incident linearly polarized beam angle in polar coordinate system. (b) top shows the reconstructed polarization angle and (b) bottom the polarization independent intensity.

sample. The measurement result can be found in Fig. 5b,c as a combination of the color-coded intensity and the polarization angle as vectors. The transmission image shows little variation except for the edges due to the low absorption of the material, but the polarization angle is strongly altered at the skewed edges up to $\pm 40^o$. The rotation of the electric field at the edges is originated in birefringent behavior. The strong anisotropy comes from a thicker zone below the contours that reinforces the mechanical structure of the sample.

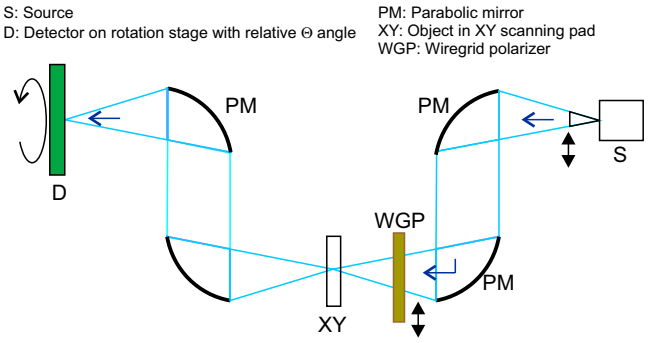

Fig. 4. (Color online) The optical setup of the polarimetric example.

In conclusion, the possibility is demonstrated that a single plasma wave detector FET with three terminal coupling is capable of measuring different radiation properties by appropriate antenna structure and current direction steering. Compared to multiple detector architectures, single device is used enabling compact detector array design. The technique could be applied also to measure interferometric patterns with interference stripes aligned to antenna arms, usable in waveform detection, or in single cycle THz wave measurements. Though the gate-source(drain) and drain-source mixing terms are not used in the application example, it may have importance of further property capturing, such as polarization ellipticity.

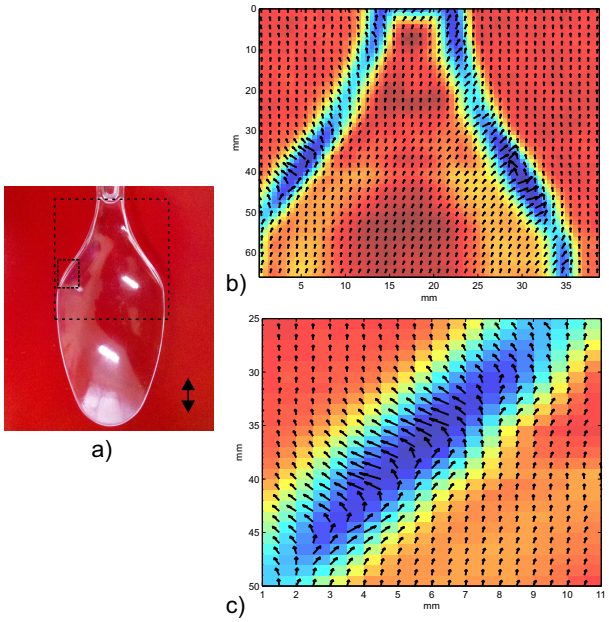

Fig. 5. (Color online) A plastic spoon has been raster scanned at $362GHz$ and the polarization independent intensity and the polarization angle are reconstructed. a) shows the visual photo of the sample showing the raster scanned areas and the source polarization direction b) and c) show the color coded intensity with overlaid polarization angles.

References

1. M. Dyakonov and M. Shur, Phys. Rev. Lett. **71**, 2465 (1993).
2. M. Tonouchi, Nat. Photonics **1**, 97 (2007).
3. W. Knap, S. Rumyantsev, M. Vitiello, D. Coquillat, S. Blin, N. Dyakonova, M. Shur, F. Teppe, A. Tredicucci, and T. Nagatsuma, Nanotechnology **24**, 214002 (2013).
4. J. Lu and M. Shur, in *Twelfth International Symposium on Space Terahertz Technology*, vol. 1 (2001), vol. 1, p. 103.
5. M. Sakowicz, M. Lifshits, O. Klimenko, F. Schuster, D. Coquillat, F. Teppe, and W. Knap, J. Appl. Phys. **110**, 054512 (2011).
6. S. Preu, S. Kim, R. Verma, P. Burke, N. Vinh, M. Sherwin, and A. Gossard, IEEE Trans. THz Sci. Techn. **2**, 278 (2012).
7. E. Castro-Camus, J. Infrared Millim. W. **33**, 418 (2012).
8. R. Zhang, Y. Cui, W. Sun, and Y. Zhang, Appl. Opt. **47**, 6422 (2008).
9. N. C. Van der Valk, W. A. van der Marel, and P. Planken, Opt. Lett. **30**, 2802 (2005).
10. E. Castro-Camus, J. Lloyd-Hughes, M. Johnston, M. Fraser, H. Tan, and C. Jagadish, Appl. Phys. Lett. **86**, 254102 (2005).
11. G. Png, S. Mickan, T. Rainsford, and D. Abbott, in *Proc. of SPIE Vol*, vol. 5649 (2005), vol. 5649, p. 769.